Available online at www.sciencedirect.com

ScienceDirect

Procedia Engineering 130 (2015) 1258 – 1272

Procedia Engineering

www.elsevier.com/locate/procedia

14th International Conference on Pressure Vessel Technology

# Assessment of Significance of Embedded Defects Caused by Cold Cracking in Welded Joints

Y. Imai[a,*], Y. Seko[a], M. Mitsuya[a], T. Hasegawa[b], S. Aihara[c]

[a]*Tokyo Gas Co., Ltd., 1-7-7 Suehiro-cho, Tsurumi-ku, Yokohama, Kanagawa 230-0045, Japan*
[b]*Nippon Steel & Sumikin Technology Co., Ltd., 20-1, Shintomi, Futtsu, Chiba 293-0011, Japan*
[c]*The University of Tokyo, 7-3-1, Hongo, Bunkyo-ku, Tokyo 113-8656, Japan*

**Abstract**

Prevention of cleavage fracture is one of the most significant problems in securing the structural integrity of welded structures. To simulate the fracture behavior and plastic constraint condition of structural components, wide-plate tensile tests have been conducted for experimental fracture assessments. Artificial surface flaws, through-wall flaws, and fatigue pre-cracks are generally applied. Embedded flaws from cold cracking should be considered in an integrity assessment of a structure. Nevertheless, experimental fracture evaluations based on wide-plate tensile tests using welded joints with embedded flaws from cold cracking have never been conducted, because a method for intentionally preparing a welded joint with a cold-cracking embedded flaw has not been established yet. In this study, we develop a means of manufacturing joints with cold cracking embedded flaws, based on the y-groove cracking test, and perform a series of cracking tests. We determine that deeper flaws crack more stably with more heat and more diffusible hydrogen. In addition, no relationship is apparent between the welding conditions (heat input/diffusible hydrogen), and the relative position of the embedded flaw to the fusion line in the cross-section. Accordingly, we establish a technique for intentionally and stably preparing a welded joint with a cold-cracking embedded flaw of sufficient height. We perform a wide-plate tensile test for the welded joint with the embedded flaw using the established technique to evaluate the fracture load and fracture behavior. The embedded flaw is found to be nearly rectangular and near the fusion line in the heat-affected zone. A fracture-origin survey of the wide-plate tensile specimen reveals that the cleavage fracture occurred from a local brittle zone at the tip of the introduced embedded flaw. Consequently, it is confirmed that this test meets the requirements for application to an evaluation on the significance of defects. Finally, we perform fracture evaluation by comparing the fracture stress with allowable stress and verify the applicability of the evaluation method using a failure assessment diagram (FAD) of the cold-cracking embedded flaw. The fracture load is found to be higher than the allowable stress; therefore, fracture will not occur even if similar embedded flaws exist in the structures. Furthermore, we confirm that a BS7910-based FAD evaluation can be applied to cold-cracking embedded flaws with a specific safety margin. Although the load observed

* Corresponding author. Tel.: +81-45-500-8737 ; fax: +81-45-505-8821.
*E-mail address:* yasu-imai@tokyo-gas.co.jp


Peer-review under responsibility of the organizing committee of ICPVT-14
doi:10.1016/j.proeng.2015.12.207

in the embedded flaw near the cross-section exceeds the plastic collapse load, the fracture load estimated by the FAD evaluation is less than the plastic collapse load. This difference can be explained by an appropriate correction of critical crack-tip opening displacement and through-thickness residual stress distribution.



Peer-review under responsibility of the organizing committee of ICPVT-14

*Keywords:* Cold cracking, Embedded flaw, Defect assessment, Welding method, Wide-plate tensile test, Allowable stress, Failure assessment diagram, HT780

## 1. Introduction

One of the most significant problems in ensuring the structural integrity of welded structures is the prevention of brittle fracture. To prevent brittle fracture, a structural integrity evaluation is conducted so that fracture will not occur from flaws that could become the origins of brittle fractures. For a structural integrity evaluation, the fracture mechanics approach [1], in which the fracture driving force and fracture toughness are compared, is typically applied. If the fracture toughness is greater than the fracture driving force, the structure is judged to be safe. Standard fracture toughness tests [2, 3] are usually performed to determine the fracture toughness of a material experimentally.. In addition, numerous wide-plate tensile tests [4, 5] have been conducted to evaluate structural integrity experimentally by precisely simulating the fracture behavior and plastic constraints of structural components.

However, some weld flaws in actual structures differ from the flaws introduced into specimens in conventional evaluation methods, as shown in Table 1. First, weld flaws in actual structures typically occur at a mid-thickness point, whereas surface flaws or through-wall flaws are typically a result of machining or possibly fatigue pre-cracking in conventional evaluation methods. In addition, realistic weld flaws tend to be distorted in shape and may not be accompanied with fatigue cracking at the weld tip, whereas in conventional evaluation methods, many well-shaped flaws resulting from machining are fatigued at the tip. It cannot be denied that these differences influence the results of a structural integrity evaluation, because both the driving force and fracture toughness can changed as a result of these differences.

Table 1. Types of flaws in wide plate specimen.

| Type of flaw for wide plate specimen | | Shape of flaw and notch root | |
|---|---|---|---|
| | | Fatigue crack from machined notch | Weld flaw |
| Location | Surface flaw | 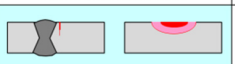 | 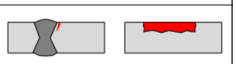 |
| | Embedded flaw | 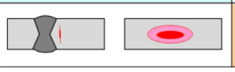 | 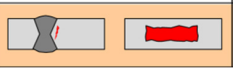 |

Although fracture evaluation using wide-plate tensile tests with realistic flaws would seem to be an effective means of evaluating the structural integrity of structural components with embedded flaws caused by weld cracking, research using this evaluation approach has never been conducted. The reason for this is that a manufacturing method capable of intentionally preparing a welded joint with an embedded flaw due to weld cracking has never been established.

In this study, we investigated the welding conditions that produce embedded flaws due to cold cracking, and set out to identify the conditions best suited for defect assessment, and then developed a method for manufacturing welded joints and intentionally introducing embedded flaws due to cold cracking, based on a series of y-groove weld cracking tests. We performed wide-plate tensile tests on welded joints manufactured according to the method developed in this study to evaluate the fracture load and fracture behavior of the joints. We performed fracture evaluations by comparing the fracture stress of the test specimens with the allowable stress, and we verified the applicability of the evaluation method using a fracture assessment diagram (FAD) for embedded flaws caused by cold cracking.

## 2. Tested Steel

The steel used to test the cracked weld areas was a high-tensile-strength steel manufactured by vacuum malting, controlled rolling, and quenching and tempering (QT), as shown in Table 2. The steel was a 780-MPa-class grade, with a nominal thickness of 25 mm. The chemical composition of the steel is summarized in Table 3, and its mechanical properties listed in Table 4. As Fig. 1 shows, the microstructure of the base metal was tempered martensite.

Table 2. Conditions of rolling and heat treatment.

| | | |
|---|---|---|
| Rolling | Controlled rolling | |
| Finishing temperature | 900 °C | |
| Target thickness | 25 mm | |
| Heat treatment | QT | |
| Quench | 930 °C, 12 min, | Water quenched |
| Temper | 625 °C, 15 min, | Air cooled |

Table 3. Chemical composition of steel tested (mass%).

| C | Si | Mn | P | S | Cu | Al | Ni | Cr | Mo | V | B | N | Ceq | Pcm |
|---|---|---|---|---|---|---|---|---|---|---|---|---|---|---|
| 0.14 | 0.24 | 0.91 | 0.008 | 0.006 | 0.31 | 0.118 | 0.09 | 1.04 | 0.48 | 0.005 | 0.0031 | 0.0137 | 0.63 | 0.31 |

$C_{eq}$(JIS,WES)=C+Si/24+Mn/6+Ni/40+Cr/5+Mo/4+V/14; $P_{cm}$=C+Si/30+Mn/20+Cu/20+Ni/60+Cr/20+Mo/15+V/10+5B

Table 4. Mechanical properties of base metal.

| YS (MPa) | TS (MPa) | EL (%) | YR (%) |
|---|---|---|---|
| 765 | 824 | 20 | 93 |

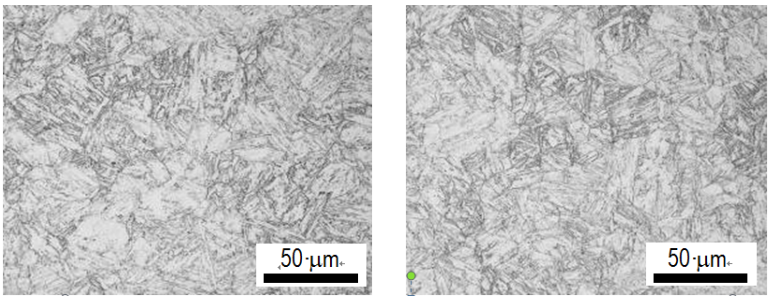


(a) 1/4 t. (b) 1/2 t.

Fig. 1. Microstructures of base metal.

## 3. Development of welded joints with embedded flaws due to cold cracking

### *3.1. Requirements for welded joints with embedded flaws due to cold cracking*

To be suitable for use in the assessment of the significance of defects, not only should it be possible to reliably obtain embedded flaws of sufficient height, but also the embedded flaws in welded joints should be introduced in such a way that the fracture origin is located in the local brittle zone of the heat-affected zone, where the toughness is heterogeneous [6]. Thus, it is desirable that cold cracking be introduced near the fusion line and be controlled so that the tip of the embedded flaw is in the coarse-grained heat-affected zone (CGHAZ). In the case of 780-MPa-

class high-tensile-strength steel, furthermore, it is even better if the material structure of the fracture origin is upper bainite, with the M-A constituent in the CGHAZ, which would enable the conservative evaluation of the toughness [7, 8].

However, it is difficult to manufacture weld joints with suitable embedded flaws that satisfy these requirements, because the relationship between cold cracking and welding conditions is unclear and the conditions under which, and the locations at which, cold cracking occurs vary. For these reasons, we chose appropriate welding conditions for the test joints after manufacturing weld cracking test specimens under a range of welding conditions and then evaluating how each embedded flaw was introduced under each set of conditions.

### *3.2. Development of manufacturing method for welded joints with embedded flaw due to cold cracking*

Cold cracking typically occurs when three conditions, namely, the presence of diffusible hydrogen, a hardened structure, and constraint stress, all exist [9]. Thus, we manufactured welded joints with embedded cold-cracking flaws under a range of conditions to ensure that the sensitivity to cold cracking would be high. The y-groove weld cracking test method specified in JIS Z 3158 [10] was used to develop the manufacturing method for welded joints. A typical weld cracking test specimen and its joint geometry are illustrated in Fig. 2. While the restraint weld has a double-V groove, in accordance with JIS Z 3158, test weld was a double-bevel groove. This joint geometry was chosen to heighten the sensitivity to cold cracking by raising the degree of constraint [11] and to facilitate the introduction of an embedded flaw at a specific location by taking advantage of the fact that diffusible hydrogen tends to be trapped near the fusion line of the flat side [12].

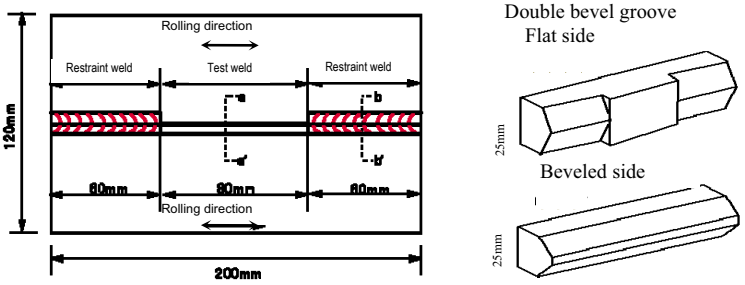


Fig. 2. Weld cracking test specimen and joint geometry.

### *3.3. Manufacture of welded joints with embedded flaws due to cold cracking*

Three specimens for each of six welding conditions for the initial layer in test welding (18 test specimens in total) were manufactured by the following procedure. First, multiple-layer welding was performed by constraint welding, according to the welding conditions shown in Table 5. Subsequently, only the initial layer of the test weld was formed. As shown in Table 6, the heat input was varied to vary the throat thickness, and the thermostatic and humidistatic chamber conditions and welding electrode conditions were varied to adjust the amount of diffusible hydrogen in the test specimens. Preheating was not performed for any of the test conditions, to heighten the sensitivity of the hardened structure to cold cracking. The test conditions were confirmed so that cold cracking would be likely to occur because the necessary preheating temperature [13], calculated from the amount of diffusible hydrogen [14], measured separately, was far higher than the normal temperature. The electrode used in the initial layer was an L-80 electrode, whereas that used in the subsequent layer was an L-60 electrode, to prevent weld cracking from the weld metal. Multiple weld layers were then formed, in the order shown in Fig. 3, from both the front and back sides, according to the welding conditions shown in Table 5. Back gouging was machined into each test weld in advance, as shown in Fig. 3, to prevent unintentional weld flaws. Fig. 4 shows an example of a weld cracking specimen manufactured in such a manner. Dehydrogenation was performed after multiple-layer welding so that the cold cracking would not extend any further.

Table 5. Welding conditions of all layers in restraint welding and subsequent layers in test welding.

| | All layers in restraint welding. | Subsequent layers in test welding. |
|---|---|---|
| Electrode | L-80 ( 4 mm) | L-80 ( 4 mm) |
| Current (A) | 180 | 180 |
| Arc voltage(V) | 24 | 24 |
| Heat input (kJ/mm) | ≈2.0 | 2.0-3.0 |
| Preheat temp. (℃) | 180 | 180 |
| Inter-pass temp. (℃) | 150~200 | 150~200 |

Table 6. Welding conditions of initial layer in test welding.

| Welding condition number | Welding current (A) | Heat input (kJ/mm) | Thermostatic & humidistatic chamber conditions | Welding electrode conditions*1 | Amount of hydrogen*2 （mL/100g） | Necessary preheat temp.*3（°C） |
|---|---|---|---|---|---|---|
| 1 | 180 | 1.93 | 20°C × RH 60% | 30°C×RH80%×24h | 9.7 | 189 |
| 2 | | 3.31 | | 400°C×1h drying | 4.0 | 135 |
| 3 | | 3.59 | | 30°C×RH80%×24h | 7.4 | 159 |
| 4 | 200 | 3.33 | 30°C × RH 80% | 400°C×1h drying | 8.6 | 166 |
| 5 | | 3.56 | | 30°C×RH80%×24h | 10.7 | 170 |
| 6 | | 3.54 | | 30°C×RH80%×2h | 9.6 | 167 |

*1 L-60 (ϕ4 mm). *2 These values are measured based on JIS Z 3118.
*3 Necessary preheat temperature for y-groove weld cracking test.

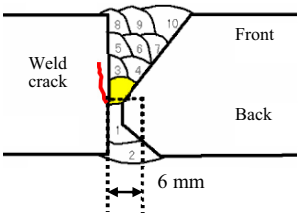


Fig. 3. Order of welding layers and outline of back.

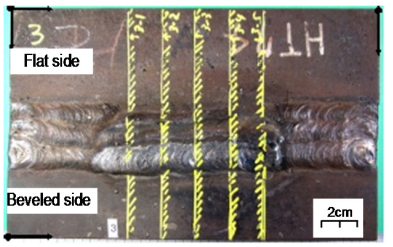


Fig. 4. Weld cracking specimen after welding.

### *3.4. Evaluation of introduced embedded flaws*

Three types of observation and evaluation of the embedded flaw in each weld cracking specimen were conducted to determine whether the specimen was suitable for use in the assessment of the significance of defects. First, we performed an ultrasonic inspection of the upper surface of the initial layer on the flat side formed before multiple-layer welding of the test weld and measured the percentage of cracking in the upper surface of the initial layer. Penetration of the cold cracking to the upper surface, which may make the precise determination of the fracture limit of a wide-plate tensile specimen with an embedded flaw difficult, had to be avoided because the tip of the embedded flaw was buried by subsequent multiple weld layers. Second, we calculated the average of five crack heights in five cross sections of the test weld, in accordance with JIS Z 3158 [10], to confirm the position and dimensions of the embedded flaw. Third, we observed each cross section macroscopically and determined the positional relationship between the embedded flaw and the fusion line.

### 3.5. Evaluation results for embedded flaws and selection of appropriate welding conditions

Figure 5 shows the cracking percentage in the upper surface of the initial layer for each welding condition. Weld cracking on the surface was detected only in the specimen corresponding to condition set 1, for which the heat input was low and the welding electrode was made to absorb moisture. This seems to be because the throat thickness of the initial layer was thin as a result of the small heat input and the cold cracking penetrating into the upper surface. On the other hand, no weld cracking was detected in the specimens with a large heat input and thick throats in the initial layer. As a result, welding conditions featuring a larger heat input were judged to be better for producing test joint welds.

Figure 6 shows the average cracking heights measured for five cross-sections and each welding condition. We successfully introduced embedded flaws caused by cold cracking for all of the conditions. Comparing the welds produced under conditions of high heat input, we found that the three specimens corresponding to condition set 5, under which the most diffusible hydrogen was measured, had the largest embedded flaws in the cross-section within the test weld. In contrast, under condition sets 2, 3, 4, and 6, the embedded flaws in the cross-sections were small and could not be reliably obtained.

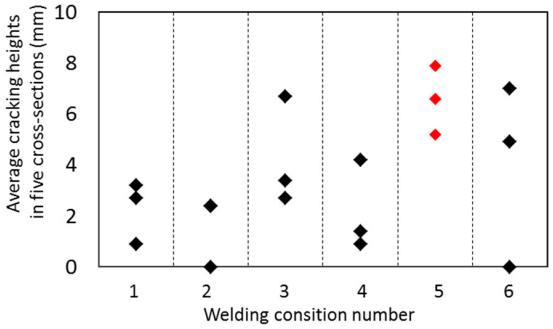


Fig. 5. Cracking percentage in upper surface of initial layer for each welding condition for each welding condition.

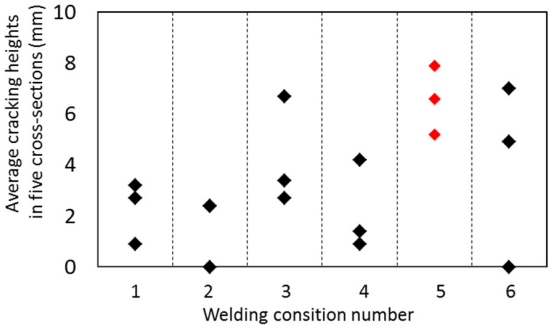


Fig. 6. Average cracking heights in five cross-sections for each welding condition.

Figure 7 shows a typical macroscopic photograph of a cross-section. Cold cracking occurred on the flat side of the groove, while no cracking was observed on the beveled side of any of the specimens. Cold cracking was observed either near the fusion line in the heat-affected zone or on the fusion line. Some specimens exhibited cold cracking at the tip in the weld metal. However, because no relationship is apparent between the welding conditions, such as the heat input and the amount of diffusible hydrogen, and the position of the embedded flaw relative to the fusion line in the cross section, it would appear to be difficult to control the position of the cold cracking in the cross-section by controlling the welding conditions.

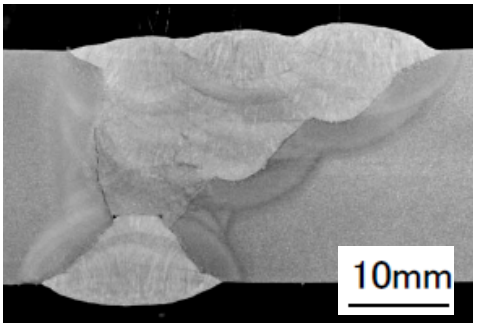


Fig. 7. Example of embedded flaw in cross-section (condition 5).

Therefore, condition set 5 (heat input: 3.0 kJ/mm; thermostatic chamber conditions: 30°C and relative humidity 80%; humidistatic chamber conditions: 30°C, relative humidity 80%, 24 h), under which the highest level of diffusible hydrogen was measured, was judged to be optimum for the welding of test joints, because this set of conditions seemed to be capable of stably producing cold cracking at a sufficient height within the test weld.

## 4. Wide-plate tensile test

### *4.1. Manufacture of specimen*

A welded joint with an embedded flaw was manufactured under condition set 5 for application to wide-plate tensile testing. While the welding procedure and conditions were almost the same as described previously, the order of welding of the layers was modified so that layers were welded in an alternating fashion from the front and back sides to minimize angular misalignment. Furthermore, as shown in Fig. 8, the back gouging procedure was modified to prevent unintentional weld cracking caused by the entanglement of slag. Accordingly, the number of passes on the back surface increased. Penetration of the cold cracking through the initial layer was not observed when an inspection of the front surface of the initial layer was performed using a liquid penetrant prior to the welding of subsequent layers of the test weld. As described previously, the welded joint was dehydrated after multiple layers had been welded.

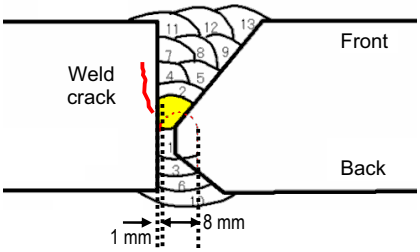


Fig. 8. Order of welding layers and outline of back gouging in test welding for wide plate tensile tests.

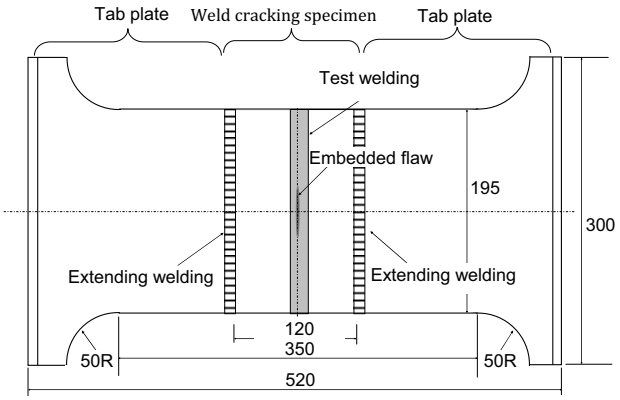


Fig. 9. Wide plate tensile specimen.

Table 7. Misalignment measured in the center.

| Angular misalignment (°) | | Axial misalignment (mm) |
|---|---|---|
| 120 mm | 520 mm | 120 mm |
| Weld cracking specimen | Wide plate tensile specimen | Weld cracking specimen |
| 0.70 | 0.15 | 0.1 |

### *4.2. Test conditions*

A 10-MN horizontal tensile machine was used for the wide-plate tensile test. The wide-plate tensile specimen was fabricated to span a distance of approximately 3100 mm between pin holes. The load, displacement, strain, and temperature during testing were measured. The displacements were measured at four points (three points on the front surface of the specimen and one point on the back surface), with gauges having a gauge lengths of 100 mm. The strains and temperatures were measured using strain gauges and thermocouples, respectively.

The test temperature was −30°C, placing it in the lower part of the ductile-to-brittle transition region in order to attain brittle fracture and incur the influence of the plastic constraint. Table 8 summarizes the mechanical properties of the base metal and the weld metal at the test temperature. The temperature at the center of the specimen was controlled to within ± 2°C by spraying liquefied nitrogen in a cooling box mounted on the center of the specimen.

Table 8. Mechanical properties at test temperature.

| T = −30°C | YS (MPa) | TS (MPa) | EL (%) | YR (%) |
|---|---|---|---|---|
| Base metal | 795 | 870 | 21 | 91 |
| Weld metal | 661 | 823 | 41 | 80 |

### *4.3. Test results*

The wide-plate tensile specimen was loaded quasi-statically at a displacement rate of approximately 0.6 mm/min until fracture. Table 9 provides an overview of the obtained test results, and Fig. 10 shows the load–displacement curve. After plastic deformation, brittle fracture occurred when the load reached 3584 kN and the average displacement reached 1.12 mm. There was no evidence of pop-in in the load–displacement curve. As Fig. 11 shows, we were able to introduce a nearly rectangular embedded flaw in the center of the specimen due to cold cracking. The embedded flaw measured a maximum of 84 mm in the welding direction and a maximum of 10.7 mm in the thickness direction. The gross fracture limit stress was 747 MPa, and the net fracture stress was approximately 847 MPa. In this way, the fracture stress of the wide-plate welded joint specimen with an embedded flaw due to cold cracking was experimentally obtained.

Table 9. Results of wide plate tensile test.

| Test temp. (°C) | Max. load (kN) | Displacement (mm) (G.L.=100mm) Position | Each | Ave. |
|---|---|---|---|---|
| −30 | 3,584 | Front, +75mm | 0.97 | 1.12 |
| | | Front, 0 mm | 1.35 | |
| | | Front, −75mm | 1.17 | |
| | | Back, 0 mm | 1.27 | |

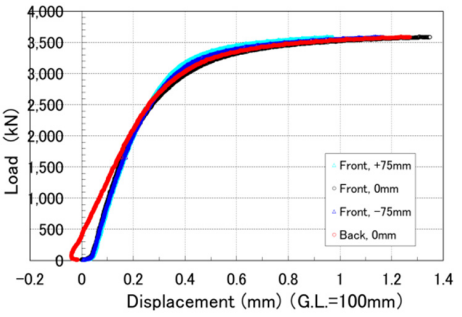


Fig. 10. Load displacement curve.

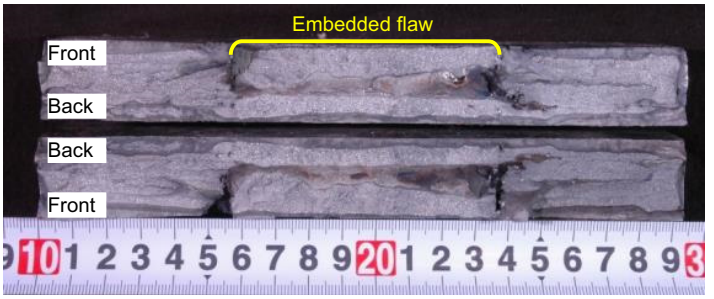


Fig. 11. Embedded flaw in the fracture surface.

### *4.4. Identification of microstructure of fracture origin*

A fracture origin survey of the fracture surface was conducted, and the microstructure of the cross-section, polished near the fracture origin, was examined using scanning electron microscopy (SEM) to confirm that the requirements stated in section 3.1 had been satisfied in the wide-plate tensile test. Fig. 12 illustrates the procedure for identifying the microstructure of the fracture origin.

The fracture origin identified in the survey is shown in Fig. 13. A stretched zone was observed between the embedded flaw and the brittle fracture surface, and the fracture origin was located at the boundary between the stretched zone and the brittle fracture surface. Unintentional welding flaws or coarse inclusions were not observed near the fracture origin. There was also no evidence of pop-in in the fracture surface.

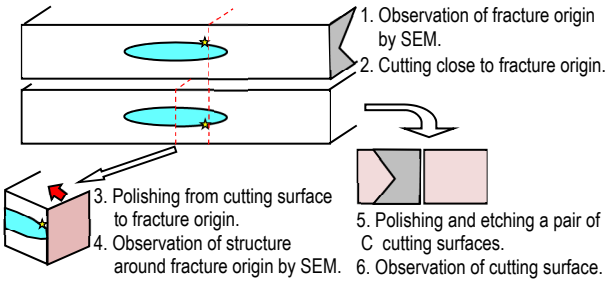


Fig. 12. Process for observation of structure around fracture origin.

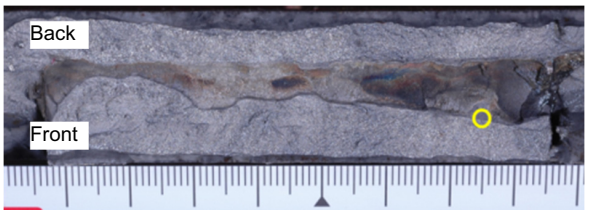


Fig. 13. Fracture origin of embedded flaw.

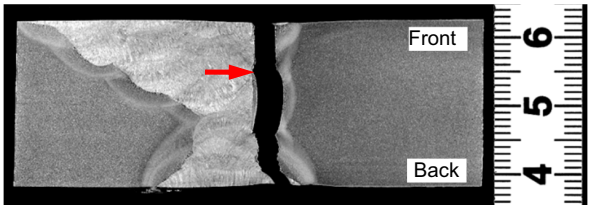


Fig. 14. Observation of cutting surface.

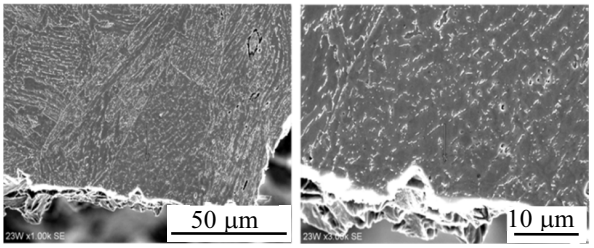


Fig. 15. Observations of structure around fracture origin by SEM.

Figure 14 shows a macroscopic photograph of the cross-section near the fracture origin, and Fig. 15 shows photographs of the microstructure of the cross-section, polished near the fracture origin, as obtained using SEM. These figures show that the embedded flaw and the fracture origin were definitely located in the heat-affected zone, near the fusion line on the flat side, that the fracture origin was located close to the fusion line (at a distance of 0.12 mm), and that the fracture origin was located in the coarse-grained heat-affected zone and consisted of upper bainite with an M-A constituent. Consequently, it was confirmed that the wide-plate tensile test of the welded joint with the embedded flaw due to cold cracking satisfied the requirements for use in the assessment of the significance of defects, because the fracture surface was in the local brittle zone.

## 5. Assessment of significance of defects

### *5.1. Comparison between critical stress and allowable stress*

We performed a fracture evaluation by comparing the fracture stress measured in the test with the allowable stress of the tested steel, to evaluate the structural integrity of welded structures with embedded flaws like that of the wide-plate tensile test specimen. The allowable stress of the tested steel, which is a 780-MPa-class high-tensile-strength steel, is 223 MPa, assuming that the allowable stress is equal to the specified minimum yield stress divided by 3.5. This value is less than half of the gross fracture limit stress, 747 MPa, mentioned in section 4.3. Accordingly, fracture will not occur even if a similar embedded flaw exists in a welded structure made of this type of steel.

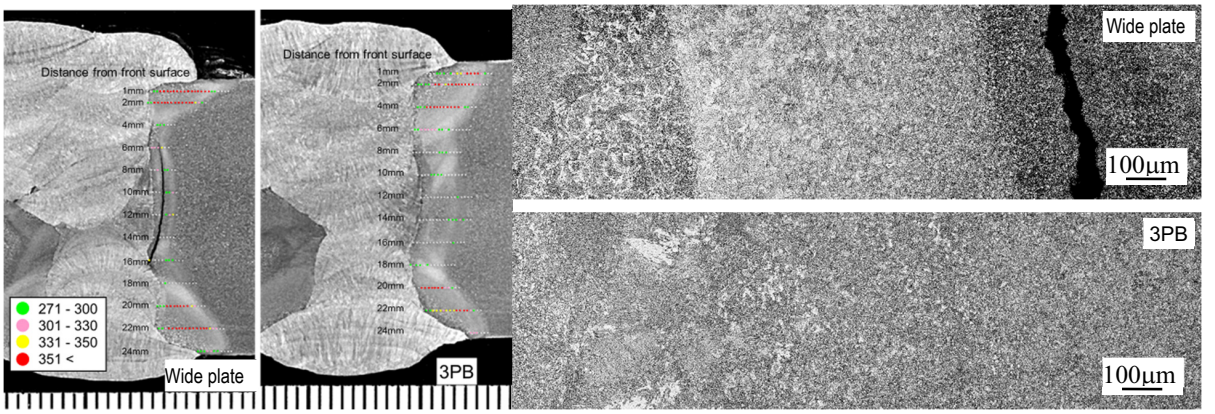


(a) Result of micro Vickers hardness tests of cutting surface (b) Structures of CGHAZ near fusion line

Fig. 16. Comparison of weld joints between wide plate tensile test and three-point bend test.

### *5.2. Assessment of significance of defect by FAD*

#### *5.2.1. Three-point bending tests for input to FAD evaluation*

The fracture stress obtained in the wide-plate tensile test was compared with a failure assessment diagram (FAD) based on BS 7910:2013[15] for an embedded flaw introduced in the wide-plate tensile test. The fracture toughness for input to the FAD evaluation was obtained in advance by three-point bending testing based on WES1108. Given the goal of manufacturing welded joints similar to the wide-plate tensile test specimen but without welding flaws, with a joint geometry and welding conditions for the welded joint used in the three-point bending test being similar to those for the wide-plate tensile test specimen, the welded joint used in the three-point bending test was manufactured with drying of the welding electrode, preheating, and precise inter-pass temperature control, in the same way as for the normal test preparation procedure. We confirmed that the hardness level and microstructure in the heat-affected zone of the tested welded joint were almost the same as those of the welded joint tested in the wide-plate tensile test, as shown in Fig. 16. After dehydrogenation, ten three-point bending tests were performed on specimens with through-wall notch thicknesses of 25 mm. The critical crack tip opening displacement (CTOD) of the four specimens for which the fracture origin was confirmed to be located in the local brittle zone, as well as that of the wide-plate tensile test specimen, were within the range of 0.059 mm to 0.162 mm.

#### *5.2.2. Inputs and results of FAD evaluation*

The input data used for the FAD evaluation are shown in Table 10. The shape of the embedded flaw was approximated by an ellipse with a diameter at the longest point of 80 mm and a width of 9 mm, such that the area of the embedded flaw and the ellipse would be identical. The measured width, thickness, and angular misalignment values were input. The strengths around the embedded flaws were heterogeneous, as shown in Table 8 and Fig. 16(a). The strength of the weld metal, considering the lowest strength of any part of the welded joint, was input from Table 8, based on the BS 7910 specification. A fracture toughness value of $K_{cr}$ = 120 MPa $\sqrt{}$m was input, based on $\delta_{cr}$ = 0.059 mm (the minimum value given in section 5.2.1). For the primary stress, a gross fracture limit stress of 747 MPa was input as the axial stress. For the secondary stress, $Q_m$ = 52 MPa and $Q_b$ = 524 MPa were input, based on the residual stress distribution in the thickness direction cited in BS 7910 Annex Q.

The results of the FAD evaluation, based on the above input values, are shown in Fig. 17. The assessment point for the fracture of the wide-plate tensile specimen with the embedded flaw due to cold cracking falls outside the failure assessment curve. This means that the FAD evaluation indicates that the specimen will fracture. Therefore, it is confirmed that the BS7910-based FAD evaluation procedure is applicable to cold-cracking embedded flaws. Furthermore, because the assessment point is quite far from the failure assessment curve, there is a specific margin of safety associated with whether the specimen will fracture.

Table 10. Input data for FAD assessment.

| Flaw detail | |
|---|---|
| Geometry | Flat plate |
| Flaw | Embedded flaw |
| Thickness (mm) | 24.6 |
| Width (mm) | 195 |
| Flaw height (mm) | 9 |
| Flaw length (mm) | 80 |
| Ligament (mm) | 7.8 |
| Angular misalignment | |
| Height of peaking (mm) | 3.8 |
| Extremities (mm) | 1000 |
| Stress ratio | 0.21 |
| Mechanical properties | |
| Yield stress (MPa) | 661 |
| Tensile stress (MPa) | 823 |
| Toughness, K (MPa√m) | 120 |
| Young's modulus (GPa) | 206 |
| Poisson's ratio | 0.3 |
| Primary stress | |
| Membrane stress (MPa) | 747 |
| Bending stress (MPa) | 0 |
| Secondary stress | |
| Membrane stress (MPa) | 52 |
| Bending stress (MPa) | 524 |

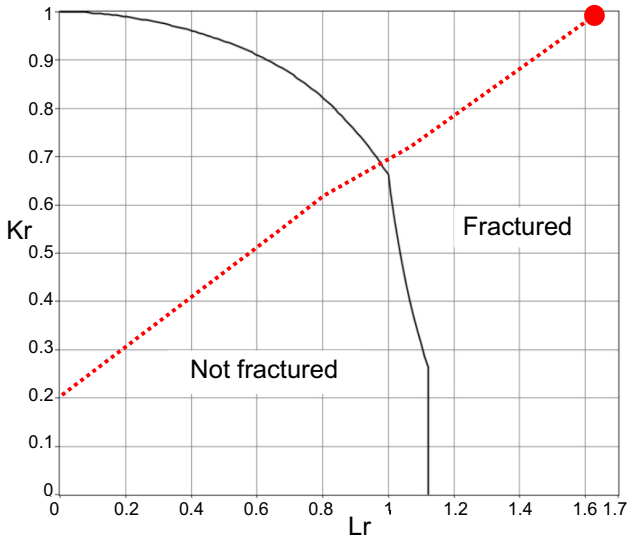


Fig. 17. Result of FAD assessment.

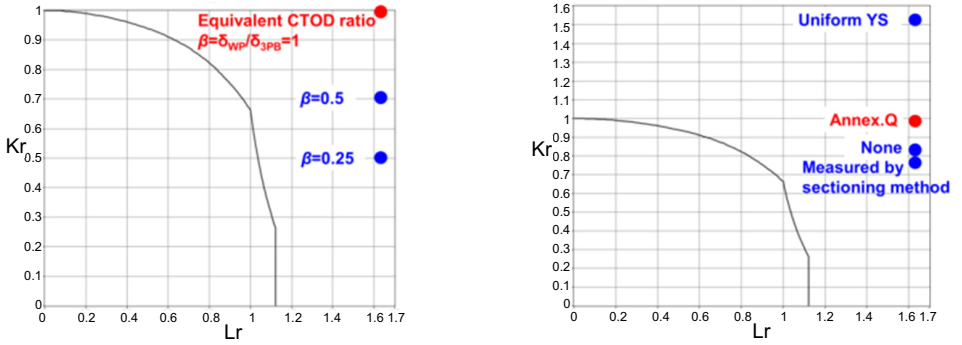


(a) Toughness (b) Residual stress

Fig. 18. Parametric study on the causes of safety margin in FAD assessment.

*5.2.3. Discussion of the failure mechanism and the safety margin*

Because the failure assessment curve used in the FAD evaluation procedure indicates the locus of the estimated failure points, it is possible to predict the fracture stress from the intersection of the failure assessment curve with the loading path showing the history of loading [16]. Next, let us consider the fracture stress of the wide-plate tensile specimen. Although the strength around the embedded flaw was heterogeneous, as shown in Fig. 16 (a), most of the ligament in the cross-section around the embedded flaw, which influences the net fracture stress, consisted of weld metal, with the lowest strength at the welded joint, as shown in Fig. 14. Considering that the wide-plate tensile specimen fractured after plastic deformation and that the net fracture stress, 847 MPa, was higher than the flow stress of the weld metal, 742 MPa, as noted in section 4.3, it is believed that the local stress in the cross-section around the embedded flaw exceeded the plastic collapse load immediately before the specimen fractured. However, the FAD evaluation results suggest that the specimen should have fractured at a fracture stress lower than the plastic collapse load.

The differences in the critical CTOD and the residual welding stress between the FAD evaluation input and the actual wide-plate tensile test are factors influencing the safety margin of the fracture stress. The critical CTOD in a three-point bending test is usually said to be lower than that in a wide-plate tensile test because of the plastic constraint [17-18]. As the notch tip of a three-point bending test specimen is introduced by fatigue cracking, while that of the wide-plate tensile specimen used in this study was introduced by cold cracking, the critical CTOD in the three-point bending test may have been lower than that of the wide-plate tensile test specimen. This is because the radius of the notch tip was smaller [19]. For this reason, the critical CTOD in the three-point bending test, which is used as an input in the FAD evaluation, can be lower than that in a wide-plate tensile test. In addition, the input values based on the distribution of the residual welding stress of the wide-plate tensile specimen, measured by sectioning the equivalent welded joint with the strain gauges on the cross-section, were Qm = -122 MPa and Qb = 396 MPa, which are lower than those based on the distribution in BS 7910 Annex Q and those used as inputs in the FAD evaluation, Qm = 52 MPa and Qb = 524 MPa. These differences may influence the FAD results.

A parametric study was conducted, varying the FAD input values for the fracture toughness and secondary stress, to assess the influence of these factors on the critical CTOD and the residual welding stress on the FAD evaluation results. The results of the parametric study are shown in Fig. 18. The assessment point in Fig. 17 is indicated in red, and the assessment points obtained by varying each parameter are indicated in blue. As Fig. 18(a) shows, as the input fracture toughness increased, considering the difference in the fracture toughness and residual welding stress, the toughness ratio Kr of the assessment point decreased. As Fig. 18(b) shows, if Qm and Qb are input based on the residual welding stress distribution measured by sectioning the equivalent welded joint with the strain gauges on the cross-section, the toughness ratio Kr of the assessment point was also smaller than the result shown in Fig. 17, which was based on the residual stress cited in BS 7910 Annex Q. In this way, the overlapping of these effects can decrease the toughness ratio Kr of the assessment point, and the loading path can cross the plastic collapse line. This means that the prediction of fracture stress by FAD corresponds to the actual fracture behavior in that the applied

stress reached the plastic collapse load before fracture in the wide-plate tensile specimen. Although FAD evaluation cannot predict the possibility of fracture after plastic collapse and cannot predict the fracture stress, it can be shown, using a reasonable critical CTOD value, corrected for the influence of the plastic constraint, the notch tip radius, and the measured residual welding stress distribution, that the wide-plate tensile specimen had already reached plastic collapse before unstable fracture.

## 6. Conclusion

Tests were conducted to determine the best conditions for the fabrication of welded joints with embedded flaws due to cold cracking for use in the assessment of the significance of defects in welded joints, and a wide-plate tensile test was conducted to evaluate the fracture load and fracture behavior of a welded joint with an embedded flaw due to cold cracking in an actual structure. The following conclusions were drawn based on the results of the study.

1) A method was developed for manufacturing welded joints with intentionally introduced embedded flaws due to cold cracking, based on the y-groove weld cracking test. Welded joints were manufactured under six different welding conditions, varying in the heat input and amount of diffusible hydrogen, to identify the best conditions for use in defect assessment, and then investigated each specimen in terms of the position and dimensions of the embedded flaws and the stability of cold cracking. As a result, the condition set (heat input: 3.0 kJ/mm; thermostatic chamber conditions: 30°C, relative humidity 80%; humidistatic chamber conditions: 30°C, relative humidity 80%, 24 h), for which the heat input was large and with the largest amount of diffusible hydrogen, seemed to reliably produce cold cracking at a sufficient height within the test weld, and therefore was chosen as the welding condition set for the wide-plate tensile test.
2) A wide-plate tensile test was performed for the welded joint with the embedded flaw under the chosen welding conditions to obtain a gross fracture-limit stress of 747 MPa and a net fracture stress of approximately 847 MPa. It was determined that the introduced embedded flaw was nearly rectangular and positioned near the fusion line in the heat-affected zone. A fracture-origin survey of the wide-plate tensile specimen revealed that the brittle fracture originated in the local brittle zone at the tip of the introduced embedded flaw. Consequently, it was confirmed that this test satisfied the requirements for application to an evaluation of the significance of defects.
3) It was determined that the fracture-limit stress was sufficiently higher than the allowable stress; therefore, fracture will not occur even if similar embedded flaws exist in the welded structures. Furthermore, it was confirmed that the BS7910-based FAD evaluation procedure is applicable to cold-cracking embedded flaws with a specific safety margin. Although the load observed in the embedded flaw near the cross-section exceeded the plastic collapse load, the fracture load estimated by FAD evaluation was less than the plastic collapse load. This difference can be explained by an appropriate correction of the critical crack-tip opening displacement and through-thickness residual stress distribution.

## Acknowledgements

The authors are grateful to Dr. Yukito Hagiwara, formerly of Sophia University and Prof. Fumiyoshi Minami and Assoc. Prof. Mitsuru Ohata of Osaka University for their valuable advice and to the IHI Corporation, the IHI Plant Construction Co., Ltd., the Osaka Gas Co., Ltd. and the Toho Gas Co., Ltd. for their support.

## References

[1] T.Kanazawa, Evaluation Methods of Fracture Toughness of Structural Steels and Significance of Defects in Welded Structures, Tetsu-to-Hagané, 64-7(1978), 990-1000. (in Japanese).
[2] BS 7448-1, Method for determination of KIc, critical CTOD and critical J values of metallic materials, British Standards Institution, (1991).
[3] WES 1108, Standard Test Method for Crack-Tip Opening Displacement (CTOD) Fracture Toughness Measurement, Japan welding engineering society, (1995), (in Japanese).

[4] H.Kihara, T.Kanazawa, H.Oba, S.Susei, S.Minakata, S.Yamamoto, Effects of Notch Size, Angular Distortion and Residual Stress on Brittle Fracture Initiation Characteristics of Welded Joints for High Strength Steels (The 2nd report), J.Soc.Nav.Archit.Jpn., 126(1970), 377-396. (in Japanese).
[5] F.Minami, M.Toyoda, Evaluation of Fracture Toughness Results and Transferability to Fracture Assessment of Welded Joints, Fatigue and fracture mechanics, 29, ASTM STP 1332 (1999), 315-340.
[6] M.Toyoda, F.Minami, Notch Orientation of CTOD Specimen for HAZ Toughness Evaluation, J.Soc.Nav.Archit.Jpn., 169(1991), 279-287. (in Japanese).
[7] J.Tsuboi, Y.Hirai, Microstructure and toughness of weld heat affected zone in quench-tempered high strength steels, J.JWS, 50-1, (1980), 28-37. (in Japanese).
[8] H.Chiba, H.Gokyu, R.Yamaba, S.Matsuda: Tetsu-to-Hagané, 71-5(1985), S590. (in Japanese).
[9] H.Matsumura, Prevention of weld crack; Cold cracking, J.JWS, 60-3, (1991), 194-199. (in Japanese).
[10] JIS Z 3158, Method of y-groove weld cracking test, Japanese Industrial Standards, (1993).
[11] K.Satoh, T.Terasaki, Effect of Joint Geometry on Stress Concentration Factor at the Root of Weld, J.JWS, 48-5, (1979), 298-303. (in Japanese).
[12] N.Yurioka, H.Suzuki, Hydrogen assisted cracking in C-Mn and low alloy steel weldments, Int.Mater.Rev, 35-4(1990), 216-249.
[13] N.Yurioka, T.Kasuya, A chart method to determine necessary preheat temperature in steel welding, Quar.J.JWS, 13-3, (1995), 347-357.
[14] JIS Z 3118, Method for measurement of amount of hydrogen evolved from steel welds, Japanese Industrial Standards, (2007).
[15] BS 7910, Guide on methods for assessing the acceptability of flaws in metallic structures, British Standards Institution, (2013).
[16] F.Minami, M.Ohata, H.Shimanuki, T.Handa, S.Igi, M.Kurihara, T.Kawabata, Y.Yamashita, T.Tagawa, Y.Hagihara: Method of Constraint Loss Correction of CTOD Fracture Toughness for Fracture Assessment of Steel Components, Eng.Fract.Mech, 73, (2006), 1996-2020.
[17] ISO 27306, "Metallic materials — Method of constraint loss correction of CTOD fracture toughness for fracture assessment of steel components," International Organization for Standardization (2009).
[18] F.Minami, T.Katou, T.Nakamura K.Arimochi, Parametric Study on Fracture Toughness Requirement Based on the Equivalent CTOD Concept, J.Soc.Nav.Archit.Jpn., 185, (1999), 293-307. (in Japanese).
[19] T.Yokobori, S.Konosu, Effects of Ferrite Grain Size, Notch Acuity and Notch Length on Brittle Fracture Stress of Notched Specimens of Low Carbon Steel, Trans.Jpn.Soc.Mech.Eng., 44-380(1978), 1114-1120.(in Japanese).